Sādhanā Vol. 28, Parts 1 & 2, February/April 2003, pp. 167–186. © Printed in India

Ductile fracture behaviour of primary heat transport piping material of nuclear reactors

S TARAFDER, V R RANGANATH, S SIVAPRASAD and P JOHRI

Fatigue & Fracture Group, National Metallurgical Laboratory, Jamshedpur 831 007, India
e-mail: star@csnml.ren.nic.in

Abstract. Design of primary heat transport (PHT) piping of pressurised heavy water reactors (PHWR) has to ensure implementation of leak-before-break concepts. In order to be able to do so, the ductile fracture characteristics of PHT piping material have to be quantified. In this paper, the fracture resistance of SA333, Grade 6 steel – the material used for Indian PHWR – under monotonic and cyclic tearing loading has been documented. An attempt has also been made to understand the mechanism responsible for the high fracture toughness of the steel through determination of the effect of constraint on the fracture behaviour and fractographic observations.

From J–R tests over a range of temperatures, it was observed that SA333 steel exhibits embrittlement tendencies in the service temperature regime. The fracture resistance of the steel is inferior in the longitudinal direction with respect to the pipe geometry as compared to that in the circumferential direction. Imposition of cyclic unloading during ductile fracture tests for simulation of response to seismic activities results in a dramatic decrease of fracture resistance. It appears, from the observations of effects of constraint on fracture toughness and fractographic examinations, that fracture resistance of the steel is derived partly from the inability of voids to initiate and grow due to a loss of constraint in the crack-tip stress field.

Keywords. SA333 steel; monotonic J–R curve; cyclic J–R curve; constraint effect; stretch zone.

1. Introduction

The design of primary heat transport piping (PHT) of nuclear reactors has to ensure that uncontrolled failure does not occur under normal, faulted or accidental service conditions. One of the most severe failure scenarios traditionally envisaged is instantaneous double-ended guillotine break (DEGB), which results in pipe-whip and consequent damage to equipment and containment. The conventional design solution to prevent such damage is to provide massive restraints to withstand pipe-whips. However, the presence of such restraints hinders efficient in-service inspection, requires additional design compensation for increased heat loss and unanticipated thermal expansion, and generally reflects an unnecessarily complex design philosophy. Over the years, with the development of a better understanding of how materials

behave, *intelligent* design of PHT systems has evolved based on the concept of leak-before-break (LBB) that precludes totally the occurrence of events such as DEGB. The LBB approach requires demonstration of the fact that PHT pipes are highly unlikely to experience sudden catastrophic rupture without prior indication of detectable leakage. LBB analysis involves the application of fracture mechanics methodology to ensure that stable ductile extension of postulated cracks or flaws in piping components, leading to *benign* leakage, occurs prior to the onset of unstable fracture. For implementation of LBB, it is therefore imperative that the ductile fracture characteristics of PHT piping material be fully understood. In this paper, the ductile fracture behaviour of SA333 Grade 6 steel – the material employed for designing PHT piping system of Indian pressurised heavy water reactors (PHWR) – is documented.

SA333 PHT piping systems conduct D_2O coolant, entering at 249°C and exiting at 293°C under 1500 psi (10·5 MPa) pressure typically. As it is a commercially produced C-Mn steel, SA333 steel may be prone to dynamic strain ageing (DSA). In fact, it has been reported that the material shows small decrease in ductility and a concomitant increase in tensile strength over the temperature range of 200–300°C (Tarafder & Ranganath 1997; Singh *et al* 1998). The variation of the fracture resistance of the steel through 28°C to 300°C has therefore been studied using the J-integral quantification, with particular attention to any manifestation of embrittlement that may be exhibited.

The integrity of components during seismic events is one of the critical issues in the design of nuclear power plants. The load fluctuation during seismic activity may be random, with postulated cracks and flaws experiencing tensile as well as compressive load amplitudes of high magnitudes leading to their extension or growth. In order to incorporate seismic factors in design, the resistance to fracture under such loading conditions must be used during LBB analysis of piping components. Fracture resistance, as quantified conventionally, is determined under essentially monotonically increasing remote loading. Since the actual resistance under seismic conditions is liable to be different, the use of cyclic J-integral tests have been proposed (Mogami *et al* 1990) to simulate the deleterious effects of periodic load reversals during monotonic tensile loading. In this paper, the fracture resistance of SA333 material obtained by such tests has been documented.

It is well-known that the fracture resistance of materials obtained from testing standard specimens is often not applicable to the fracture of components made of that material due to the difference in the constraint or triaxiality conditions at the tip of the crack in the two cases (Kirk *et al* 1993). In order to obtain an appreciation of the nature of variation of fracture resistance of SA333 steel with variation of constraint, a study has been conducted employing specimens with various initial crack lengths so as to impose a systematic variation of constraint. From the results of the study, and extensive fractographic characterisation of the fracture surface produced by the fracture tests, an attempt has been made to understand the origin of the high level of toughness of the SA333 steel.

2. Material and experimental details

The SA333 Grade 6 steel employed for the investigation was supplied by the Bhabha Atomic Research Centre, Mumbai. Most of the tests were conducted on specimens fabricated from sections of PHT pipes of 406 mm (16") OD and 31 mm wall thickness. For some constraint effect tests, smaller specimens machined from 203 mm (8") OD pipes (15 mm thickness) were also used. The nominal composition of the SA333 steel is given in table 1. Table 2 lists the mechanical properties of the material of the two sizes of pipes obtained from tensile tests at

Table 1. Chemical composition of SA333, Grade 6 steel in wt%.

C	Mn	Si	S	P
0·18	0·90	0·25	0·02	0·02

room temperature. The tensile flow curve of the steel exhibited prominent yield-point effect accompanied by non-hardening strain propagation (Lüders strain) of $\sim$ 2%.

Being a C-Mn steel, the microstructure of the SA333, Grade 6 steel was heavily banded. Figure 1 shows the typical microstructure of the steel consisting of bands of pearlite in a ferritic matrix. Banding was observed on the circumferential as well as axial transverse cross-section of pipes, indicating that the pearlitic phase was arranged spatially in three-dimension along concentric cylinders. It was also noticed that the intensity of banding increased towards the inner surface of the pipe. The steel was relatively clean, with an average inclusion volume fraction of 0·094%.

Compact tension (CT) specimens, of 25 mm thickness (B) and 50 mm width (W), were employed for carrying out monotonic J–R tests at room temperature, 200, 250 and 300°C, and for cyclic J–R tests at room temperature. For studying constraint effects on ductile fracture behaviour, single-edge notched bend (SENB) specimens were preferred due to the unacceptable distortions that occur at the loading holes of the CT geometry for lower initial crack lengths. Three SENB specimen sizes were used: $W = 25$ mm, $B = 8$ mm; $W = 25$ mm, $B = 8$ mm; and $W = 50$ mm, $B = 25$ mm. The constraint effect tests were conducted only on specimens in the L–C orientation with respect to the pipe geometry, i.e. with a transverse crack growing circumferentially. Monotonic and cyclic J–R tests were carried out with L–C as well as C–L (transverse crack growing longitudinally) specimens. All specimens were equipped with integral knife-edges, either on their front face or at the load-line (in case of CT), for compliance based crack length measurement, and were side-grooved after fatigue pre-cracking. Specimens were fatigue pre-cracked under decreasing ΔK envelopes in servohydraulic testing systems interfaced to computers for test control and data acquisition.

The single-specimen technique was employed for generating J–R curves as per the procedures laid down in ASTM standard E1820 (ASTM 1999). The loading scheme for this technique consisted of ramping pre-cracked specimens at a rate of 3×10^{-3} mm/s through constant incremental displacements, followed by unloading and then reloading through 50% of the incremental displacement at the same rate, and repeating the sequence 20 to 25 times till substantial crack extension had taken place through ductile tearing. A typical load-displacement record that results due to the implementation of this scheme is shown in figure 2(a). It may

Table 2. Mechanical properties of SA333, Grade 6 steel at room temperature.

Material	YS(MPa)	UTS(MPa)	% El	% RA
Pipe, 8" dia	292	429	36·2	76·64
Pipe, 16" dia	307	463	39·1	76·15

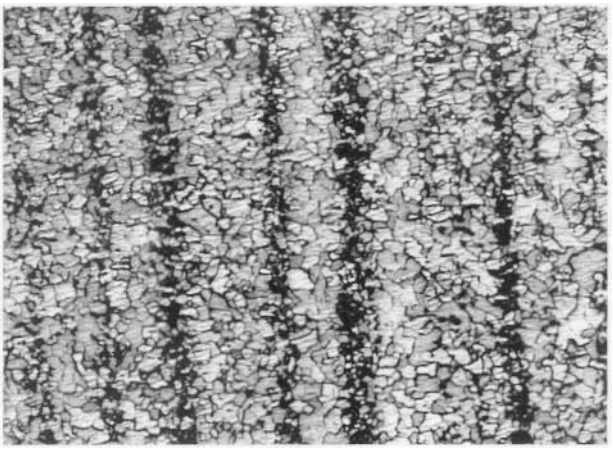

Figure 1. Typical microstructure of the SA333, Grade 6 steel (300 X).

be noted that the displacement axes in figure 2 represent load-line displacement (LLD), suitably corrected for load-point indentation (for SENB). The crack length a at each instance of unloading was calculated from the elastic compliance C of the unloading curve using compliance crack length relations of the form

$$a/W = f(u), \quad u = 1/[(EBC)^{1/2} + 1], \tag{1}$$

where E is the elastic modulus and f is a polynomial function. For the CT specimen geometry, the compliance was corrected for rotation of the displacement measurement location during testing. The energy parameter J for the instant of ith unloading was calculated incrementally using

$$J_{(i)} = [K_{(i)}^2(1 - \nu^2)/E] + J_{pl(i)}, \tag{2a}$$

$$J_{pl(i)} = \left[J_{pl(i-1)} + \left(\frac{\eta_{(i-1)}}{W - a_{(i-1)}}\right)\frac{\Delta A_{pl(i)}}{B_N}\right] \cdot \left[1 - \gamma_{(i-1)}\frac{a_{(i)} - a_{(i-1)}}{W - a_{(i-1)}}\right]. \tag{2b}$$

In the above equations, $K_{(i)}$ is the stress intensity factor, calculated from the instantaneous load $P_{(i)}$ and the crack length $a_{(i)}$; ν is the Poisson's ratio; η and γ are geometry and crack length dependent factors; $\Delta A_{pl(i)}$ is the incremental area under the load-plastic LLD curve of the ith loading displacement; and B_N is the net specimen thickness obtained after side-grooving. The second term of (2b) represents the correction proposed by Joyce & Link (1997) to account for crack extension in the loading step. The η and γ factors in (2b) are strongly dependent on crack length and were obtained from relations given by Sumpter (1987). This is particularly necessary when pre-crack lengths are varied through a large range in order to study constraint effects on ductile fracture.

The load, displacement and crack mouth opening displacement (CMOD) data obtained from ductile fracture tests were analysed post-test employing a software to obtain a set of J and crack extension, Δa, data pairs that constituted the J–R curve. The software incorporated iterative procedures for obtaining the experimental blunting line slope m, the power law representation of the tearing part of the resistance curve, and the adjusted initial crack length a_{oq}. This ensured that subjectivity in determination of critical parameters such as the fracture toughness J_c, obtained at the intersection of the power law tearing curve with the offset

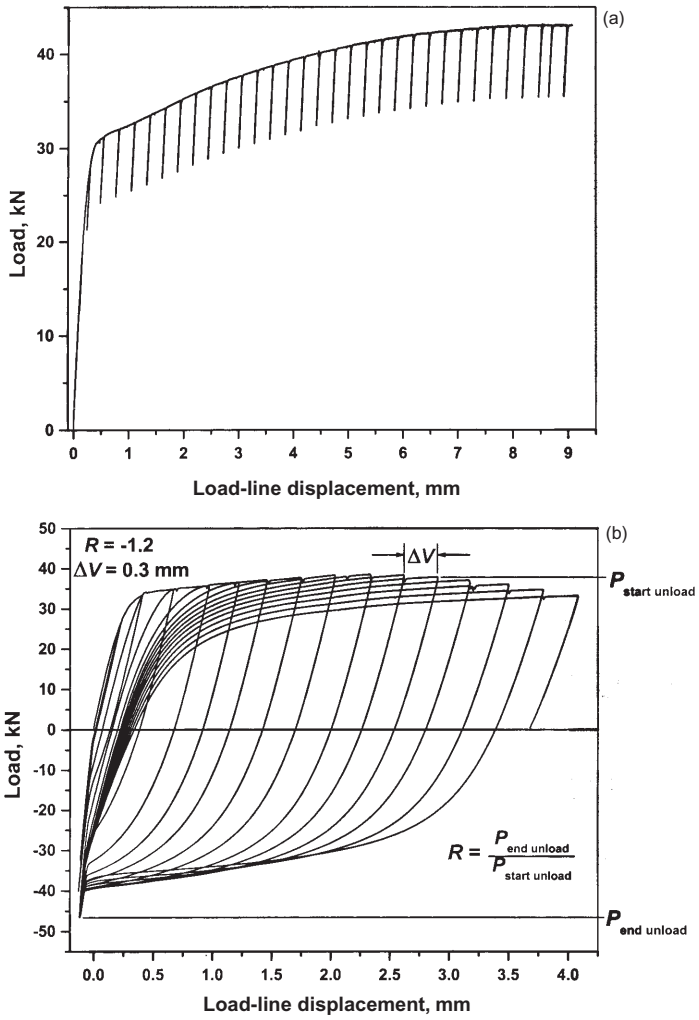

Figure 2. Typical load-displacement records obtained in **(a)** monotonic J–R testing, and **(b)** cyclic-J testing.

blunting line at $\Delta a = 0{\cdot}2$ mm, was eliminated. Comparison of J–R curves from tests with small amount of variation in test parameters, like initial crack length or test temperature, was also facilitated due to this.

The concept of cyclic J–R tests is of recent origin, and there is controversy over the applicability of the J-integral to compressive crack tip load excursions that take place in such tests. However, just as in the case of the single-specimen technique for monotonic J–R curve determination in which violation of the theoretical definition of J through crack extension and periodic unloading was accepted in favour of an engineering solution by consensus (Landes *et al* 1979), an understanding is likely to emerge with respect to the credibility of cyclic J–R as well. In this investigation, the procedure adopted for conducting cyclic J–R tests was exactly the same as that for conventional single-specimen monotonic J–R tests, except for the fact that the periodic unloading were continued up to load levels determined by the unloading

load-ratio R of the test, defined as the ratio of the minimum load achieved by unloading to the load from which unloading was initiated. Tests were conducted at ambient temperature. Incremental loading displacement ΔV of 0·15, 0·3 and 0·5 mm were used, and for each ΔV, R of 0, −0·5, −0·8, −1 and −1·2 were employed. ΔV can be taken to represent the frequency of recurrence of cyclic unloading during a seismic event, while R is a quantification of the magnitude of the cyclic amplitude of such unloading, so that the test matrix encompasses a wide variety of seismic activities.

A typical load-LLD plot obtained from a cyclic J–R test is shown in figure 2b. R and ΔV are schematically defined in the figure. The difference between the loading pattern in a cyclic J–R test and a monotonic J–R test is immediately evident on comparison with figure 2a. For calculation of crack length in cyclic J–R tests, only the linear portion of the unloading curve was used. J was calculated from the area under the envelope curve above the baseline $P = 0$ (which is equivalent to the procedure adopted for monotonic J–R tests). The software used for analysis of monotonic J–R tests was adapted for analysis of cyclic J–R test data.

Some of the fracture surfaces produced through the various categories of ductile fracture tests were observed under the scanning electron microscope. Particular attention was paid to record the stretch zone that forms ahead of the fatigue pre-crack prior to the tearing extension of the crack through the process of microvoid coalescence.

3. Results and discussions

3.1 *Elevated temperature fracture resistance*

J–R curves of SA333, Grade 6 steel obtained from tests at 28, 200, 250 and 300°C are shown in figures 3a and b for L–C and C–L orientations of crack growth respectively. It is immediately apparent from the figure that there is almost no effect of increase in temperature on the fracture resistance of the steel for circumferential crack extension (L–C), the J–R curves for the various temperatures being nearly superimposed on each other. On closer inspection, the resistance curve for 250°C may appear to be consistently lower than the other curves. However, the difference is so marginal that it can be considered as insignificant. For axial crack extension (C–L) on the other hand, there seems to be a lowering of the resistance to fracture on increase of temperature, reaching a minimum at 250°C followed by a small recovery at 300°C. Normally, with increasing temperatures, the fracture resistance of materials increases due to the enhancement of the plastic deformation capacity of the material (Lepik & Mukherjee 1990), unless consequent embrittlement mechanisms are triggered. The very fact that in the L–C orientation fracture resistance does not improve with temperature indicates that embrittling mechanisms are operative. This proposition is strengthened by the behaviour exhibited in the C–L orientation – fracture resistance being lowered progressively up to 250°C. The improvement exhibited in the J–R behaviour at 300°C for the C–L orientation is also characteristic of embrittlement phenomena, which are often active over a range of temperature.

The effect of temperature on the J–R behaviour of SA333 steel must be viewed in light of the variation of its tensile properties with temperature. Figure 4 shows the effect of temperature on the tensile strength and % elongation of SA333 steel (Singh *et al* 1998). Normally in steels the strength decreases and ductility increases with increasing temperature. However, in the case of the SA333 steel under investigation, it can be seen from figure 4 that there is deterioration in % elongation, and a corresponding increase in strength, in the temperature range of 200–300°C. Although the magnitude of change is small, this is an unmistakable sign

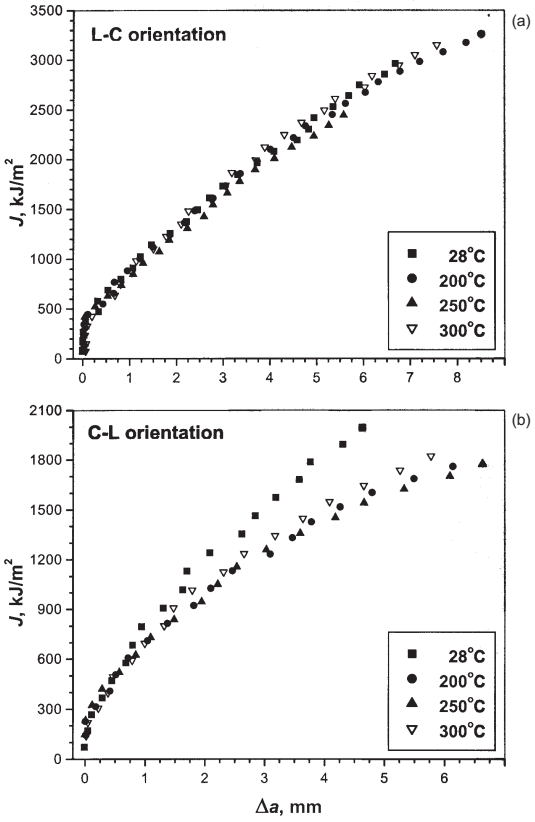

Figure 3. J–R curves of SA333, Grade 6 steel obtained from tests at various temperatures for **(a)** L–C and **(b)** C–L orientations of crack growth.

of embrittlement of the steel over that temperature range. It may be mentioned that the yield stress of the material decreases continuously up to 300°C, as is to be expected. Based on the tensile deformation response of SA333 steel at elevated temperatures it can be said that the

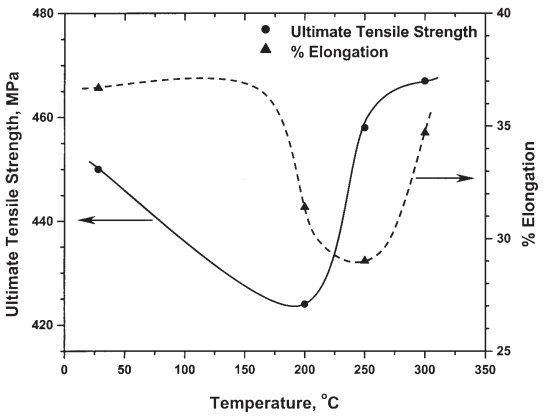

Figure 4. Effect of temperature on the tensile strength and % elongation of SA333 steel.

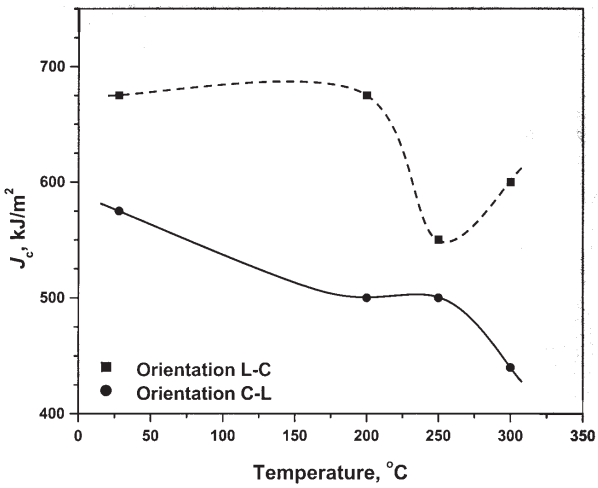

Figure 5. Variation of the critical toughness J_c with temperature for L–C and C–L orientation of crack extension.

embrittlement tendency of the steel is appropriately reflected in the temperature sensitivity of its J–R behaviour. This tendency can be quantifiably represented by the variation of the critical toughness J_c, obtained from the J–R curves in figure 3, with temperature, as shown in figure 5. Note in particular that J_c for the L–C orientation exhibits a minimum at 250°C with a slight recovery at 300°C, similar to the pattern displayed by the J–R curves for the C–L orientation. This reinforces the conclusion that SA333 suffers an embrittlement and consequently exhibits deterioration in its fracture resistance through 200–300°C. It must be pointed however that the embrittlement is not severe. Particularly for the L–C orientation, representing the direction of postulated flaws that experience the highest stresses in service, there is no lowering of the J–R curve. At the same time, the fact that the embrittlement temperature range encompasses the operating temperature of PHT piping of nuclear reactors calls for stringent LBB analysis of piping systems.

3.2 *Cyclic J–R behaviour*

The execution of cyclic J–R tests was fraught with a number of engineering problems, not the least of which was imposing periodic compressive load excursions on the pin-loaded CT specimen. However, since displacements were measured locally at load-line knife-edges on the specimen, backlash in the loading train during load traverse through zero did not affect the test data adversely.

It is to be expected that imposition of high amplitude unloading cycles during monotonic fracture tests will aid in the process of fracture. However, the effects revealed by cyclic J–R tests were truly dramatic. Figure 6 summarises the effect of variation of R on J–R curves of SA333 steel. It can be seen that on increase in the (negative) magnitude of R, for a constant tearing displacement ΔV, the fracture resistance of the steel is significantly compromised, with the effect saturating beyond $R = -1$. Compared to the J–R curve for $R = 0$, the tearing modulus of that for $R = -1$ is almost four times lower. Similarly, the initiation toughness can be estimated to be 2-3 times lower for the latter in comparison to the former. It is thought that the damage produced in the fracture process zone at the crack tip by each cyclic unloading is so large that crack extension ensues readily on resumption of tensile loading. A probable manifestation of this damage is the initiation of excess voids, which grow and participate in

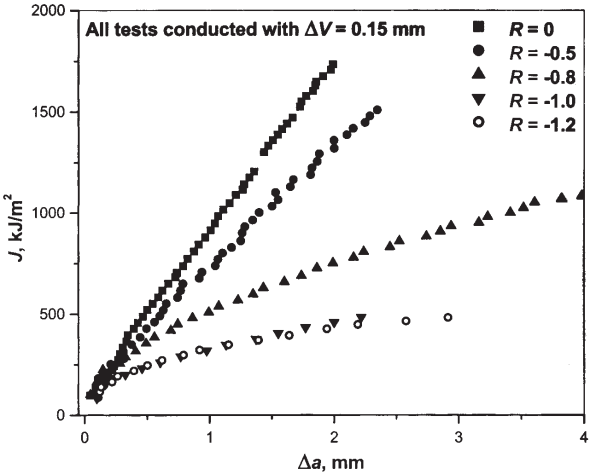

Figure 6. Effect of variation of cyclic unloading stress ratio R on J–R curves of SA333 steel for tests conducted with ΔV of 0·15 mm.

the crack extension process. Additionally, crack extension is facilitated by the re-sharpening of the blunted crack tip by compressive excursions of the load during cyclic unloading. The saturation of cyclic unloading effects at highly negative R-ratios is presumably due to the complete closure of the crack at such levels of unloading, leading to transfer of load through the crack faces in preference to compressive deformation at the crack tip. This is corroborated by the fact that fracture surface features are almost completely obliterated for such high unloading R-ratios.

If each cyclic unloading excursion in cyclic J–R tests is responsible for incorporating substantial amount of damage so that effectively the fracture resistance is overcome easily, then it is logical to assume that increasing the frequency of cyclic unloading will enhance the process. Decrease of ΔV essentially increases the frequency of unloading, and the effect of variation of ΔV on the J–R curve is shown in figure 7 for R-ratios of 0, $-0{\cdot}8$ and $-1{\cdot}2$. The sub-plots in figure 7 have the same axes scaling in order to facilitate visual comparison of effects at different R. It can be seen from figure 7 that the effect of frequency of unloading is dependent on the extent of unloading, characterised by R. For $R = 0$, there seems to be no effect, presumably because cyclic unloading with positive R-ratios, i.e. those that do not impose compressive loads, have almost no effect on the J–R behaviour. For highly negative R-ratios at which cyclic unloading effects saturates, e.g. for $R = -1{\cdot}2$, again the effect of variation of ΔV is minimal. This is probably due to the fact that during each cyclic unloading at highly negative R, the fractional damage incorporated into the fracture process zone at the crack tip is near unity, and, unless the crack is extended beyond this zone by sufficient tearing displacements, further cyclic unloading does not appreciably enhance the damage-state. For intermediate R-ratios ($R = -0{\cdot}8$ in figure 7), ΔV has a significant effect, with more frequent cyclic unloading (or a smaller ΔV) causing greater deterioration as expected. The frequency of cyclic unloading together with the extent of unloading thus seems to have a synergistic effect on J–R behaviour.

All the cyclic J–R data presented in figures 6 and 7 were obtained from specimens in the L–C orientation. The cyclic J–R behaviour of SA333 steel in the C–L direction of crack extension is essentially similar. A comparison of the effect of specimen orientation on cyclic J–R curve is given in figure 8 for two cyclic unloading R-ratios at a constant incremental

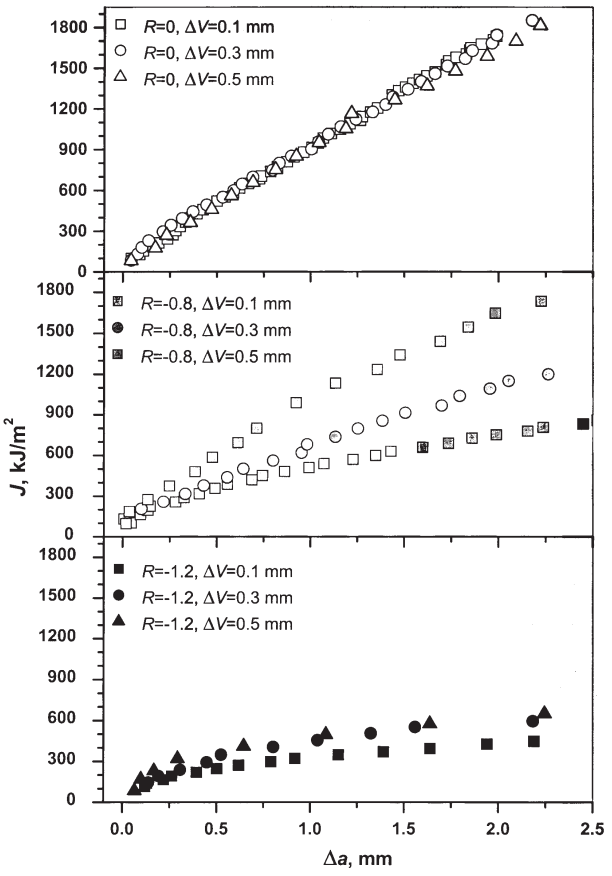

Figure 7. Effect of variation of ΔV on the J–R behaviour of SA333 steel for cyclic unloading R-ratios of 0, −0·8 and −1·2. Note that the axes of the sub-plots have identical scaling for easy comparison.

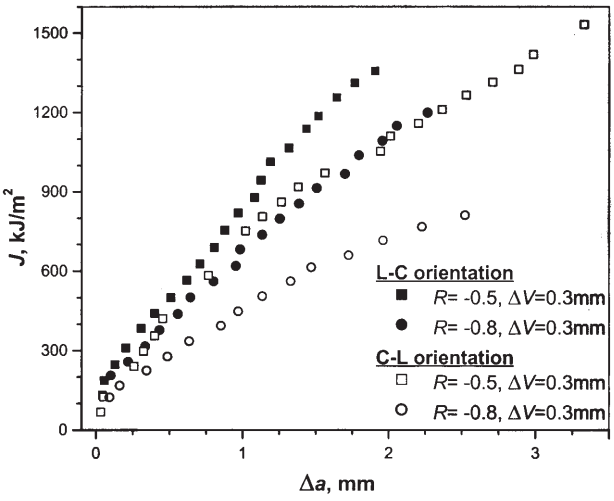

Figure 8. Comparison of the effect of specimen orientation on cyclic J–R curves of SA333 steel.

displacement. It can be seen from the figure that the fracture resistance in the C–L orientation (open symbols) is lower than that in the L–C orientation (closed symbols). This behaviour is consistent with the fracture resistance observed under monotonic J–R tests, as can be observed from a comparison of the resistance curves in figures 3a and b and the initiation toughness in the two orientations shown in figure 5.

Attempts have been made to model the J–R behaviour under cyclic loading through additive computations using fatigue crack growth data and monotonic J–R data (Joyce 1986; Marschall & Wilkowski 1991). Such techniques are however questionable because cyclic unloading occurring during cyclic J–R tests are of variable plastic amplitudes often with negative R-ratios, and conventional fatigue data have to be extrapolated considerably for characterising the fatigue component. Synergistic interactions between the effects produced by frequency of unloading and extent of unloading, as observed in the present investigation, also cannot be rationalised in an additive framework without resorting to empiricism. The success of such techniques has therefore been selective, and a reliable generalised basis for modelling cyclic J–R curves is yet to evolve. Some researchers have advocated that J be computed for cyclic J–R tests from the area under the load-LLD curve and above the crack opening load (Dowling & Begley 1976), which corresponds to the cusp in the unloading curve at $P < 0$. The rationale for such an argument being that once the crack is fully open, the energy expended in further opening it directly contributes to crack tip processes that are responsible for crack extension. In this investigation, however, such a procedure is not followed, essentially because it is considered that cyclic J–R tests are a special case of monotonic J–R tests, and because it is sought to be established how a quasi-static monotonic J–R curve is modified due to periodic cyclic unloading as during cyclic J–R tests.

3.3 *Effect of constraint on fracture resistance*

Conventionally fracture toughness of ductile materials and their fracture resistance curves are determined using deep-cracked specimens with $a/W \approx 0{\cdot}5$ in order to ensure that the crack tip is positioned in a highly constrained bending field. Specimens are also required to possess sufficient thickness so that predominantly plane strain conditions exist at the crack tip. Under these conditions, the stress field at the crack tip may be assumed to follow the Hutchinson-Rice-Rosengren (HRR) asymptotic field so that it can be uniquely characterised by the J-integral parameter. Standard methods of testing thus ensure that a structure-insensitive measure of fracture toughness and fracture resistance under high constraint is obtained. In real structures, cracks may often not be subjected to high constraint, e.g. shallow surface cracks. Often the specimen size obtainable from a structure may not be able to simulate the constraint condition to which cracks in the structure are subjected. For piping components made of SA333 steel both these scenarios are applicable.

If the crack length in a specimen is varied widely, the constraint condition at the crack tip can be made to vary, meaning that the stress field at the crack tip will deviate from the HRR field. This deviation will be dependent not only on the crack length but also on the specimen geometry and even on the loading level vis-à-vis the deformation behaviour of the specimen material. To quantify the deviation, proposals of using one (or more) additional parameter together with J have been forwarded, most popular of which is the J–Q theory (Gullerud & Dodds 1995). For understanding the response of the SA333 steel to variation of constraint, J–R curves were obtained from the three sizes of SENB specimens pre-cracked to a/W in the range 0·2 to 0·6 in steps of $\sim$ 0·05. Results from the set of specimens with $W = 25$ mm, $B = 8$ mm are shown in figure 9. With small variation in a/W, the J–R curve changes only very slightly, and hence nearest pairs are grouped together in each sub-plot of figure 9 for clarity. Selected J–R curves

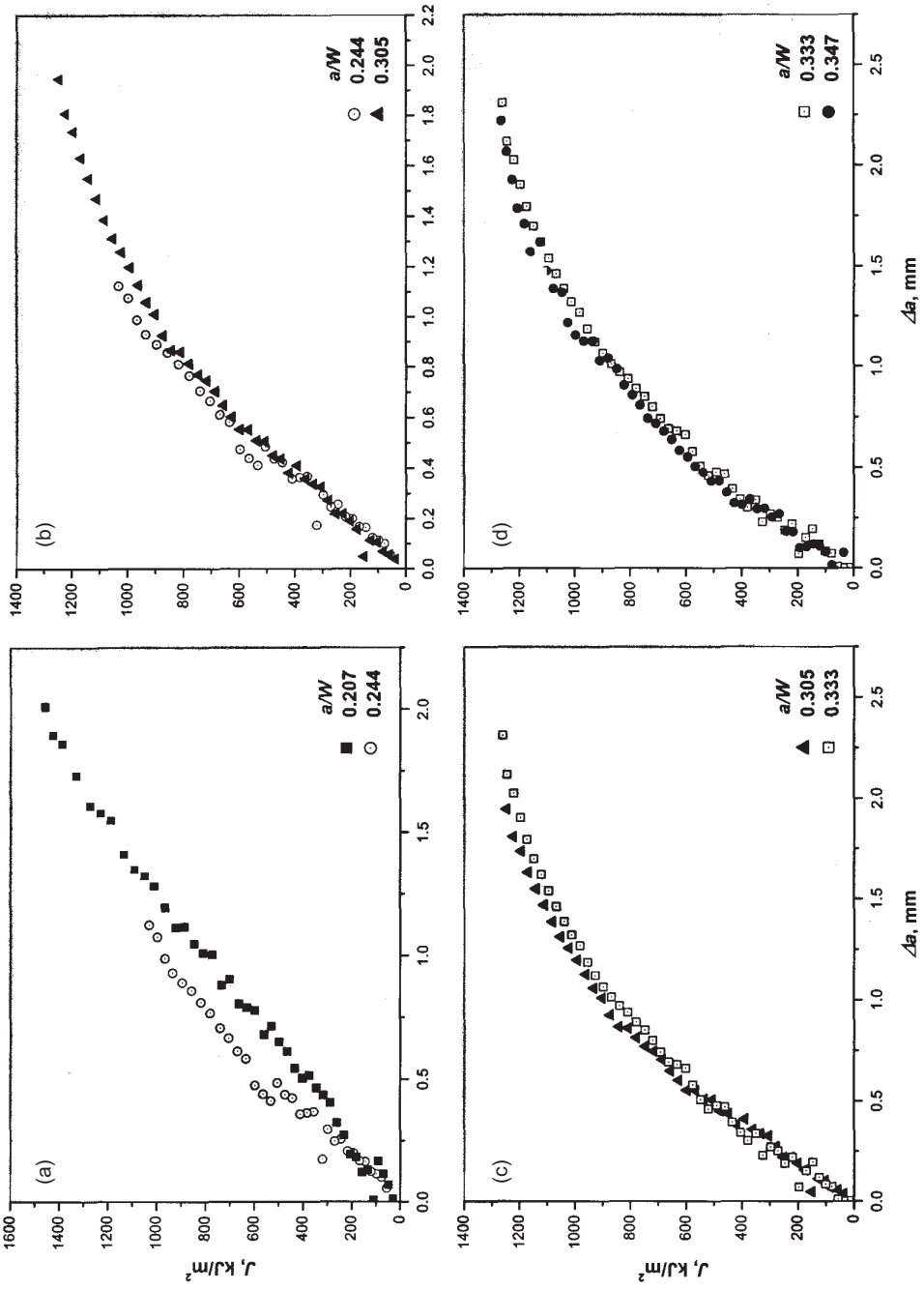

Figure 9. (Caption on facing page.)

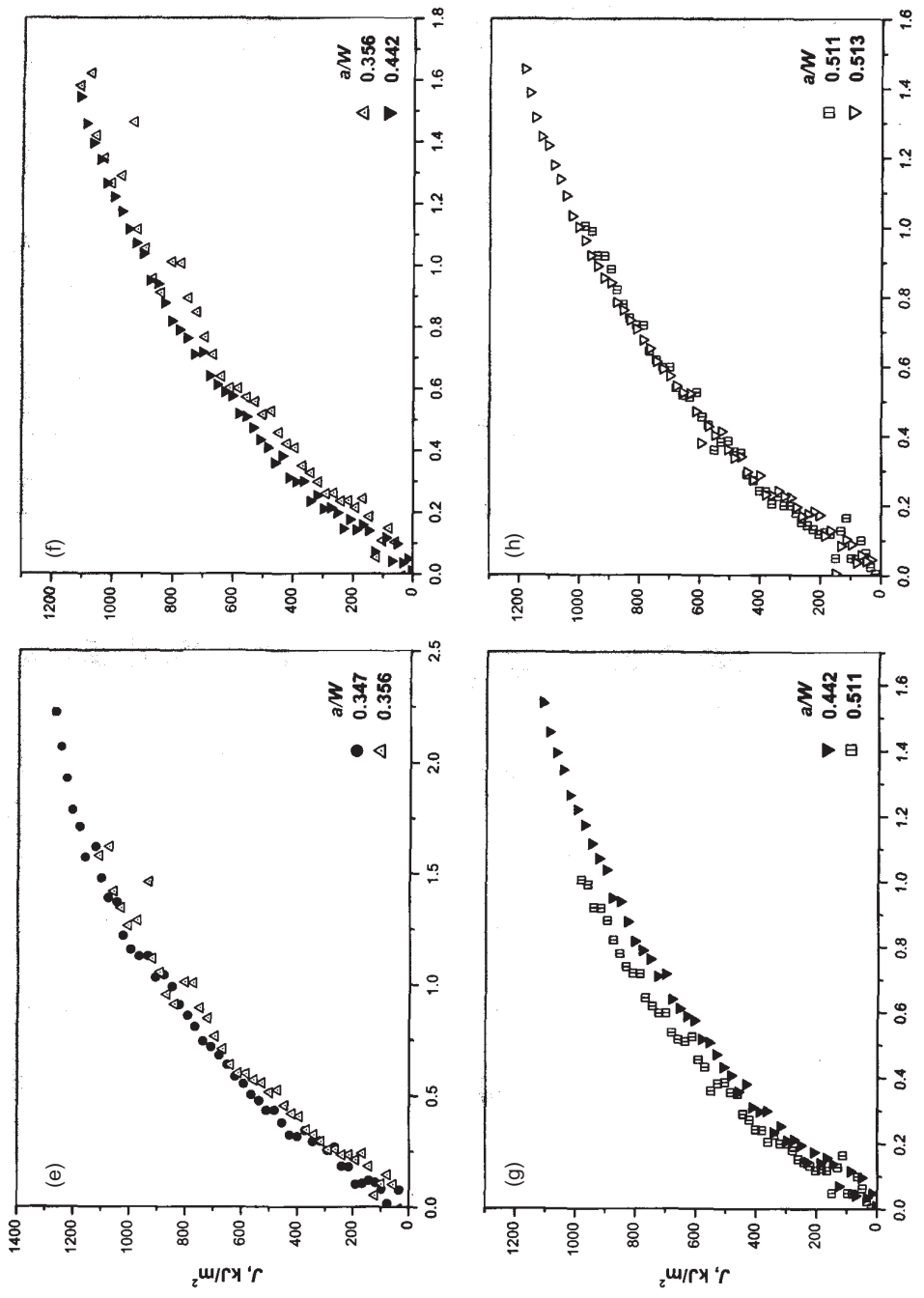

Figure 9. (contd.) J–R curves of SENB specimens of $W = 25$ mm, $B = 8$ mm size and varying initial a/W. Nearest pairs are grouped together in each sub-plot.

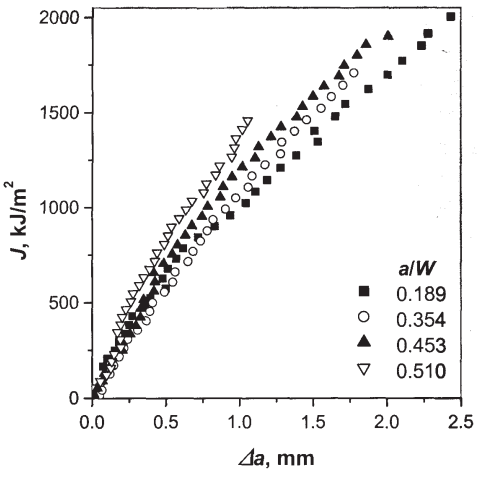

Figure 10. Selected J–R curves obtained from SENB specimens of $W = 50\,\text{mm}$, $B = 25\,\text{mm}$ size.

obtained from $W = 50\,\text{mm}$, $B = 25\,\text{mm}$ specimens are shown in figure 10. On examination of figures 9 and 10, it is clear that a generalised trend for the effect of constraint on the J–R behaviour of SA333 steel cannot be formulated. It is more instructive to look at the nature of variation of critical toughness J_c derived from the J–R curves. Determination of J_c from J–R curves that differ only slightly requires the use of a robust method that precludes any subjectivity. The iterative technique based on the procedures of ASTM standard E1820 (ASTM 1999) that has been incorporated in the analysis software was particularly useful in this regard. Figure 11 shows the effect of crack length variation on J_c for all the three sizes of SENB specimens.

It has been shown (Kikuchi 1997) that enhancement of constraint results in the lowering of fracture toughness. Conversely, a loss of constraint (i.e. depression of the crack tip stress field to below that given by the HRR solution) increases the experimentally determined fracture toughness. For SA333 steel, a similar situation exists at lower a/W values, as can be seen from figure 11. On increase of a/W, J_c decreases, signifying an improvement in the

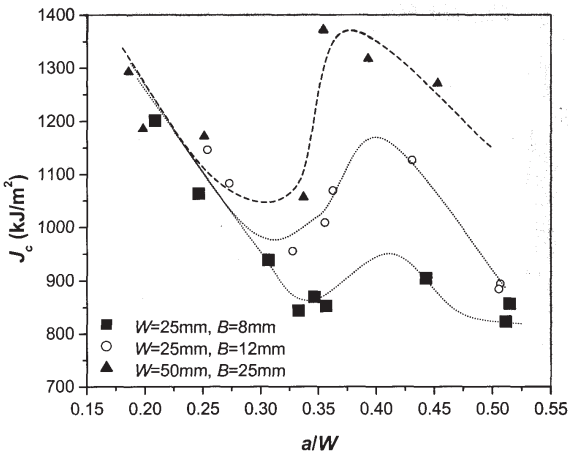

Figure 11. Effect of variation of crack length on J_c for three sizes of SENB specimens.

constraint. However, in all the three sizes of specimens, there appears to be a recovery in the fracture toughness around $a/W \approx 0{\cdot}35$, which peaks before decreasing again at higher crack lengths. It is believed that this behaviour is due to a renewed loss of constraint as a result of yielding of the remaining ligament. It can thus be inferred that determination of fracture toughness in SA333 steel using standard specimens with $a/W \approx 0{\cdot}5$ can result in abnormally high values pertaining to a low constraint condition, even for the biggest size of specimen ($W = 50$ mm, $B = 25$ mm) obtainable from PHT pipe geometries. It may be pointed out, with reference to figure 11, that contrary to conventional wisdom, fracture toughness at higher crack lengths appears to increase with increasing specimen thickness. However, since the stress triaxiality at crack tips under such conditions is thoroughly of plane stress type, this behaviour is to be expected.

3.4 *Mechanism of ductile fracture resistance*

In spite of tendencies of embrittlement at temperatures comparable to service temperature of PHT piping, and notwithstanding the fact that under seismic loading conditions its fracture resistance may be severely compromised, SA333, Grade 6 steel can be said to possess an excellent fracture toughness. At the basic level, this superior fracture resistance stems from the microstructure of the steel and its deformation behaviour, the cleanliness and excellent ductility of the steel being major parameters in this regard. From a fracture mechanics point of view, the high fracture toughness of SA333 steel can be said to be originating from the blunting behaviour of cracks and loss of constraint at the crack tip on loading. The loss of constraint experienced by SA333 fracture toughness specimens has been discussed in the previous sub-section. The nature of the process of crack tip blunting in the steel is reviewed below.

In ductile materials, sharp fatigue pre-cracks blunt on the application of load in order to accommodate plastic strains arising out of the local deformation process at the crack tip. On continuation of loading, the blunting at the crack tip reaches a limiting size, governed by the deformation capabilities of the material, and further initiates a fracture (ductile crack) at its tip that extends by the process of microvoid coalescence. On a ductile fracture surface, crack tip blunting is manifested as a featureless region known as the stretch zone. The stretch zone that forms during the process of ductile fracture can be thought of as a frozen imprint of the state of deformation at the instant of the critical event of ductile crack extension. The dimensions of the stretch zone can therefore be correlated to the fracture toughness irrespective of the size and geometry of the specimen, as shown by Roos & Eisele (1988).

In SA333 Grade 6 steel, it was observed that the ductile fracture surface consists of a series of ridges. figure 12 shows a low magnification view of the entire ductile fracture surface of a fracture toughness specimen in which the ridge-and-valley relief of the fracture is obvious. In order to reveal the fractograhic features that constitute the typical relief, a series of fractographs were acquired along the centreline of a specimen. A montage of such fractographs is shown in figure 13. The figure is annotated appropriately to indicate the various features and their characteristics. It may be noted from the figure that stretch zone features appear repeatedly in the valleys. In an ideal ductile fracture, crack extension through void coalescence is preceded by a single expanse of stretch zone. It is therefore surprising to note the formation of multiple stretch features in the SA333 material.

As mentioned earlier, the stretch zone essentially forms to accommodate the plastic strains that are required for void growth ahead of the crack. Once the process of crack extension through coalescence of voids with the blunted crack tip is initiated, continual extension of

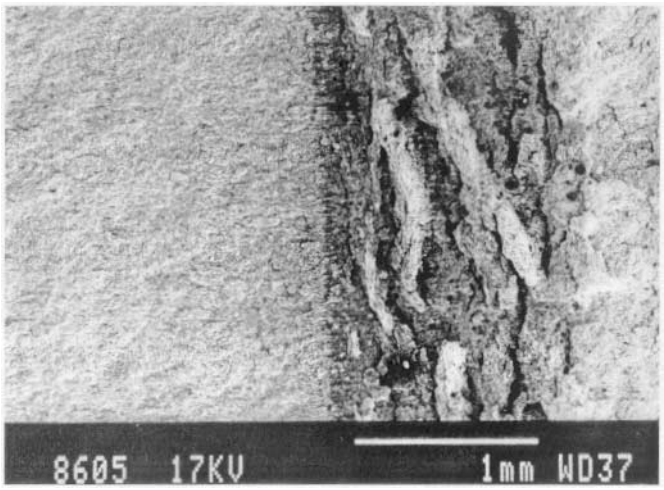

Figure 12. Low magnification view of the entire ductile fracture surface of a fracture toughness specimen of SA333 steel.

the crack by the same process is assured due to the availability of matured voids further ahead. The repeated formation of stretch zones in the SA333 material indicates that after the first initiation of ductile crack extension by the usual process, mature voids are not available ahead of the crack to result in continued growth through coalescence. This may happen if sufficient strains have not been accumulated in the far field of the crack. Considering the evidence of drastic loss of constraint even in deeply cracked specimens of the steel, such a situation is plausible. Further strain accumulation through the formation of a stretch zone therefore becomes necessary in order to induce sufficient void growth ahead of the current crack tip.

Although there is lack of clarity in defining which is the stretch zone in the SA333 steel, it may be argued that the dimension of the first expanse of stretch features can be used to obtain J_{str} from the J–R curve. J_{str} is identified at $\Delta a = \Delta a_{str}$, the width of the stretch zone. It has been shown by Roos & Eisele (1988) that J_{str} is identical to J_i, which is obtained at the departure of the J–R curve from the blunting line. Such an exercise was attempted for the steel and it was observed that (i) there is confusion in measurement of even the first expanse of stretch due to the presence of discontinuous ridges, and (ii) the J_{str} obtained is much smaller than J_i. figure 14 depicts the problems associated with measuring the first expanse of stretch zone. It is obvious from the figures that the first expanse of stretch is highly non-uniform along the thickness of the specimen. In such situations, a large number of measurements have to be made at various points along the crack front, and an average value used. Such a procedure was adopted for a few specimens in order to ascertain the suitability of J_{str} in unambiguously identifying J_i. figure 15 compares the J_{str} obtained by the averaging procedure with the J_i obtained graphically for a SENB specimen with $W = 50$ mm and $B = 25$ mm. It is clear that J_{str} is much less than J_i.

The unsuitability of J_{str} in representing the initiation toughness of the SA333 steel may be explained in light of the hypothesis proposed earlier for the formation of the ridge-and-valley fractographic relief. While ductile crack extension initiates at J_{str}, continued extension of the crack through microvoid coalescence process is not possible because of the unavailability of matured voids under the impoverished stress triaxiality due to the loss of constraint. The applied J has to be increased considerably to J_i in order to induce the development and

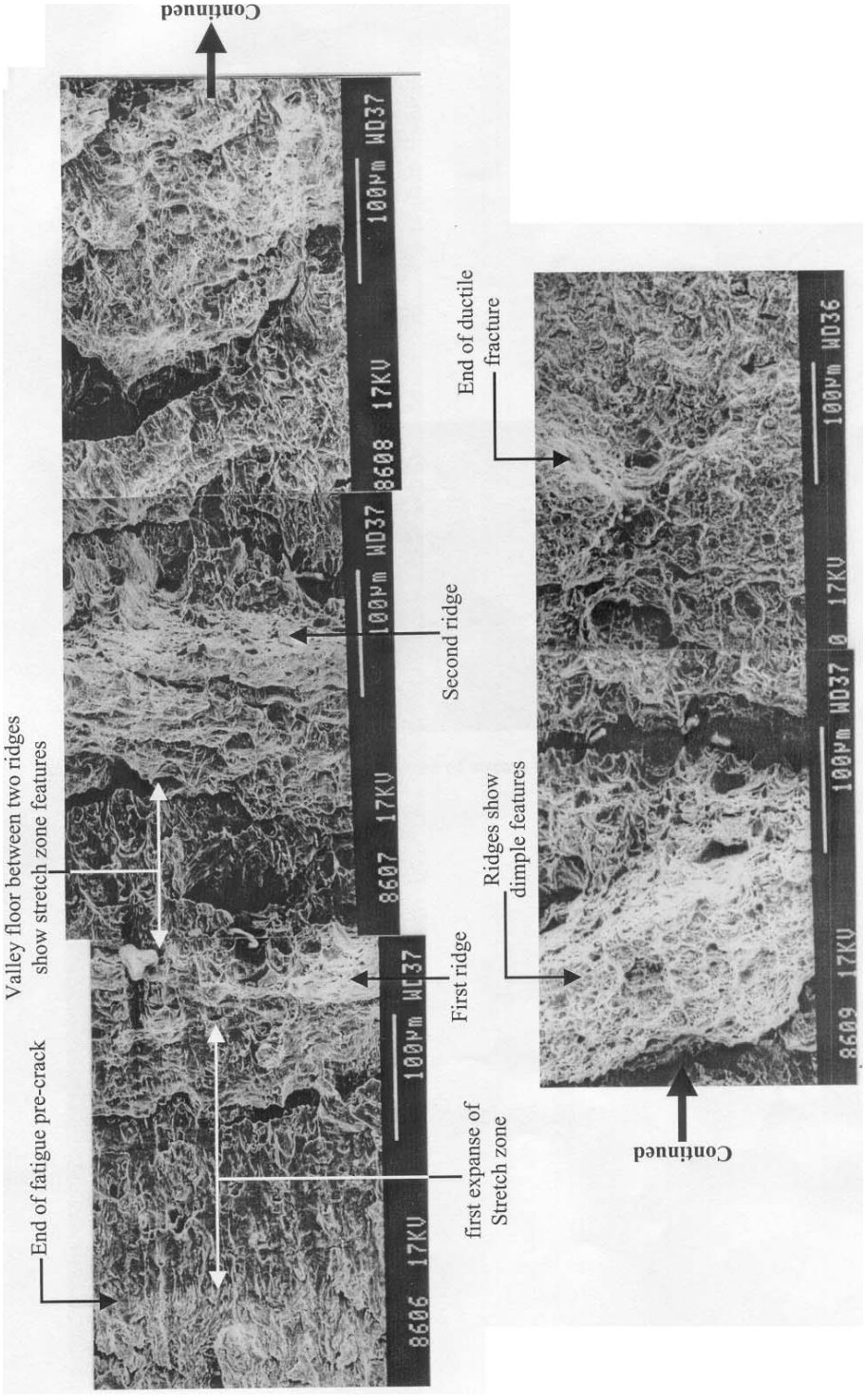

Figure 13. Montage of fractographs obtained along the centreline of a fracture toughness specimen.

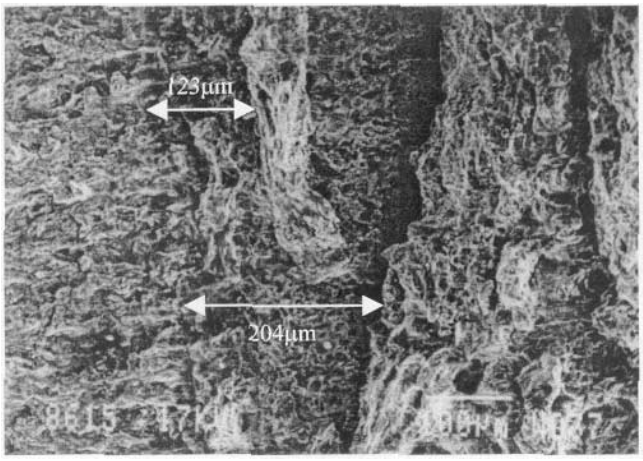

Figure 14. Non-uniformity of the first expanse of stretch zone observed on fracture surfaces of SA333 steel.

coalescence of voids so as to ensure continuous growth of the crack. The crack therefore extends and blunts a number of times, evolving, in the process, the typical ridge-and-valley fractographic features. In fact, it may be thought that the repeated blunting of cracks in SA333 steel, and the consequent formation of ridge-and-valley fractographic features, is actually a mechanism of increasing the toughness of the material.

4. Conclusions

In this paper, an overview of the ductile fracture behaviour of SA333, Grade 6 PHT piping steel subjected to monotonic and cyclic loading, and under variation of crack tip constraint conditions, has been presented.

The fracture resistance of SA333 steel has been evaluated at various temperatures up to 300°C for crack extension in the circumferential and longitudinal direction with respect to

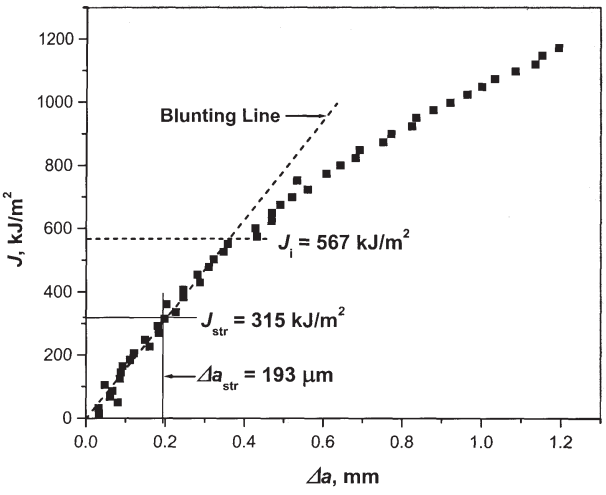

Figure 15. Comparison of J_{str}, obtained from stretch zone measurements, with J_i, obtained graphically at the departure of the R-curve from the blunting line, for SENB specimen ($W = 50$ mm, $B = 25$ mm) of SA333 steel.

the piping geometry. It was established that fracture resistance of the steel was inferior in the longitudinal direction, and that the steel exhibited evidences of embrittlement in the temperature range of 200–300°C. The manifestation of embrittlement on the fracture resistance curve, however, was not extensive.

In contrast, the fracture resistance of SA333 steel suffered drastic reductions upon imposition of periodic compressive cyclic unloading in simulation of ductile fracture during seismic events. The contribution of non-compressive cyclic unloading was found to be minimal. A synergistic effect of the frequency of unloading and the extent of unloading was observed.

From the study of variation of constraint on fracture behaviour, it was evident that even for the maximum size of standard specimen obtainable from SA333 piping components, a loss of constraint occurred during fracture toughness testing. This leads to a high fracture toughness being determined for the material. In fact loss of constraint seems to be a mechanism through which steels of this class inhibit ductile crack extension.

Fractographic characterisation of ductile fracture surfaces has shown that ductile crack extension through microvoid coalescence is suppressed in SA333 steel due to the absence of adequate stress triaxiality at the crack tip that supports and promotes void generation and growth. The crack tip in this material therefore has to repeatedly blunt in order to accommodate the increased strains necessary for void initiation, leading to an exhibition of a ridged fracture surface.

The studies on elevated temperature fracture behaviour and constraint effects on fracture were supported by contracts from the Bhabha Atomic Research Centre, Mumbai (BARC). The study on cyclic J–R behaviour of SA333 steel was supported by a research grant from Board of Research in Nuclear Sciences. The Reactor Safety Division of BARC provided the material necessary for conducting the studies.

References

ASTM 1999 *E1820-99, Standard test method for measurement of fracture toughness* (Philadelphia, PA: ASTM)

Dowling N E, Begley J A 1976 Fatigue crack growth during gross plasticity and the J-integral. *Mechanics of crack growth* ASTM STP 590, (Philadelphia, PA: ASTM) pp 82–103

Gullerud A S, Dodds R H 1995 J–Q and toughness scaling model solution for M(T), DE(T), SE(B), SE(T) and C(T) specimens. *Int. J. Fracture* 72: R11–R21

Joyce J 1986 Development of a criterion for the effect on J–R curve of elastic unloading, *Proc. 18th Symposium on Fracture Mechanics* (eds) D T Read, R P Read, ASTM STP 945 (Philadelphia, PA: ASTM) pp 647-662

Joyce J A, Link R E 1997 Application of two parameter elastic-plastic fracture mechanics to analysis of structures. *Eng. Fracture Mech.* 57: 431–446

Kikuchi M 1997 Study on the effect of the crack length on the J_{IC} value. *Nucl. Eng. Design* 47: 41–49

Kirk M T, Koppenhoefer K C, Shih C F 1993 Effect of constraint on specimen dimensions needed to obtain structurally relevant toughness measures. *Constraint effects in fracture* (eds) E M Hackett, K-H Schwalbe, RH Dodds, ASTM STP 1171 (Philadelphia, PA: ASTM) pp 79–103

Landes J D, Walker H, Clarke G A 1979 Evaluation of estimation procedures used in J-integral testing. *Elastic-plastic fracture* ASTM STP 668 (Philadelphia, PA: ASTM) pp 266–287

Lepik O E, Mukherjee B 1990 Ductile fracture properties for assessing LBB issues in ferritic weldments. *Int. J. Press. Vessel Piping* 43: 285–300

Marschall C W, Wilkowski G M 1991 Effect of cyclic loading on ductile fracture resistance. *J. Press. Vessel Tech. (Trans. ASME)* 113: 358–364

Mogami K, Hayashi T, Ando K, Ogura V 1990 Elastic-plastic FCG and tearing instability behaviour under cyclic loads. *Int. J. Press. Vessel Piping* 44: 85–97

Roos E, Eisele U 1988 Determination of material characteristic values in elastic-plastic fracture mechanics by means of J-integral crack resistance curves. *J. Testing Eval. JTEVA* 16: 1–11

Singh P K, Chattopadhyaya J, Kushwaha H S, Tarafder S, Ranganath V R 1998 Tensile and fracture properties evaluation of PHT system piping material of PHWR. *Int. J. Press. Vessel Piping* 75: 271–280

Sumpter J D G 1987 J_c determination for shallow notch welded bend specimens. *Fatigue Fracture Eng. Mater. Struct.* 10: 479–493

Tarafder S, Ranganath V R 1997 Investigation on elevated temperature J–R behaviour of nuclear grade piping steel. Report No. F&F/BARC/JR/P2, National Metallurgical Laboratory, Jamshedpur